Research Paper

Improved Tumor Uptake by Optimizing Liposome Based RES Blockade Strategy

Xiaolian Sun,[1,2] Xuefeng Yan,[2] Orit Jacobson,[2] Wenjing Sun,[1] Zhantong Wang,[1,2] Xiao Tong,[2] Yuqiong Xia,[2] Daishun Ling,[3] Xiaoyuan Chen[2]✉

1. State Key Laboratory of Molecular Vaccinology and Molecular Diagnostics & Center for Molecular Imaging and Translational Medicine, School of Public Health, Xiamen University, Xiamen 361102, China.
2. Laboratory of Molecular Imaging and Nanomedicine (LOMIN), National Institute of Biomedical Imaging and Bioengineering (NIBIB), National Institutes of Health, Bethesda, Maryland 20892, United States.
3. Zhejiang Province Key Laboratory of Anti-Cancer Drug Research, College of Pharmaceutical Sciences, Zhejiang University, Hangzhou, 310058, China.

✉ Corresponding author: shawn.chen@nih.gov.

Abstract

Minimizing the sequestration of nanomaterials (NMs) by the reticuloendothelial system (RES) can enhance the circulation time of NMs, and thus increase their tumor-specific accumulation. Liposomes are generally regarded as safe (GRAS) agents that can block the RES reversibly and temporarily. With the help of positron emission tomography (PET), we monitored the *in vivo* tissue distribution of ^{64}Cu-labeled 40×10 nm gold nanorods (Au NRs) after pretreatment with liposomes. We systematically studied the effectiveness of liposome administration by comparing (1) differently charged liposomes; (2) different liposome doses; and (3) varying time intervals between liposome dose and NR dose. By pre-injecting 400 μmol/kg positively charged liposomes into mice 5 h before the Au NRs, the liver and spleen uptakes of Au NRs decreased by 30% and 53%, respectively. Significantly, U87MG tumor uptake of Au NRs increased from 11.5 ± 1.1 %ID/g to 16.1 ± 1.3 %ID/g at 27 h post-injection. Quantitative PET imaging is a valuable tool to understand the fate of NMs *in vivo* and cationic liposomal pretreatment is a viable approach to reduce RES clearance, prolong circulation, and improve tumor uptake.

Key words: Reticuloendothelial system, Nanoparticle, Liposome blockade, Positron Emission Tomography, Enhanced tumor uptake.

Introduction

The surge of nanotechnology has led to notable advancements in the field of oncology [1-3]. Nanomaterials (NMs), with large surface areas, unique properties, and tunable signal outputs, are great candidates for cancer theranostics [4-5]. Unlike small molecules, NMs can passively target solid tumor tissue due to the enhanced permeation and retention (EPR) effect [6-7]. After intravenous administration, they circulate in the vascular system, preferentially penetrate into tumor tissue *via* leaky tumor blood vessels, and tend to retain in the tumor bed due to a lack of effective lymphatic drainage. However, many NMs can be sequestered by the reticuloendothelial system (RES) and cleared rapidly from the circulation before they reach the tumor. This nonspecific sequestration not only causes a decrease in tumor-specific accumulation (a median of 0.7% of the administered NMs reach solid tumors based on a literature survey over the past 10 years [8]), but also raises concerns of possible damage to RES-rich organs such as the spleen and liver [9].

Many attempts have been made to minimize the sequestration of NMs by RES macrophages. One approach is to optimize the physicochemical properties of NMs such as size, charge, and surface coating [10-12]. However, this approach may attenuate their original signal output and tumor targeting capabilities. For example, although PEGylated ultrasmall silica NMs are renally cleared with low RES accumulation, the tumor targeting

efficiency is only around 1.0 to 1.5 %ID/g, much lower than conventional NMs [13, 14].

Another approach is to preemptively suppress RES macrophage activity. A variety of materials that are toxic to macrophages including dextran sulfate 500, methyl palmitate, and gadolinium chloride have been pre-injected into mice to deplete macrophages in order to increase the blood circulation of a secondary injection of NMs [15-18]. Nevertheless, the possibility of systemic toxicity for these agents is of great concern.

Liposomes as drug carriers have been used as Trojan horses to help deliver these suppressors specifically into macrophages [19-21]. Meanwhile, it has been found that pre-injection of empty liposomes may saturate macrophages reversibly, and thus decrease liver uptake of a subsequent dose of similar vesicles with little to no side effect on the liver function [22]. Since the RES clearance process of inorganic particles resembles the clearance route of liposomes, the "RES blockade" phenomenon induced by pre-administration of empty liposomes may also be applicable to inorganic NMs. However, considering its controversial effectiveness, the "liposome based RES blockade" strategy has not been extensively explored for other NMs. In a recent study, this approach has successfully decreased subsequent RES uptake of 25 nm iron oxide nanoclusters and resulted in a near 2-fold enhancement of MRI signal in the tumor area [23]. Although this study provided visible evidence of the benefits, it is still unclear how this strategy could affect the tissue distribution of a subsequent dose of NMs. It is thus highly desirable to obtain detailed information on the comparative pharmacokinetics and distribution of NMs with and without this approach, as this will guide future design and optimization of dosing strategies for maximal tumor enrichment of NMs.

In this study, we pre-administered empty liposomes to reduce RES clearance in an effort to improve the tumor uptake of a second dose of gold nanorods (Au NRs). Au NRs are one of the most widely used NMs in the theranostic field [24]. A recently developed direct ^{64}Cu labeling method, without the need for macrocyclic chelator, was utilized in our study [25, 26]. With the help of ^{64}Cu based positron emission tomography (PET) imaging, Au NR distribution can be monitored continuously and noninvasively. We thoroughly investigated the effect of liposome administration including: (1) injection of liposomes with different charges; (2) variation of liposome dose; (3) modulation of the time interval between liposome dose and NR dose. After optimizing the procedure for pre-injection of liposomes, the liver and spleen uptake of the second

Au NR dose successfully decreased by 30% and 53% respectively, while the tumor uptake increased by 50%.

Materials and Methods

Chemicals and Materials

1,2-Dipalmitoyl-*sn*-glycero-3-phosphocholine, 1,2-dipalmitoyl-sn-glycero-3-phosphoglycerol, and 1,2-dipalmitoyl-3-trimethylammonium-propane were purchased from Avanti Polar Lipids (Alabaster, AL, USA). Au NRs (40 × 10 nm) were purchased from Nanopartz (Loveland, CO, USA). Poly(ethyleneglycol)-thiol (MW 5000 g/mol) was purchased from Nanocs (New York, NY, USA). 1,4,7,10-tetraazacyclododecane-1,4,7-triyl)triacetic acid (DOTA) was purchased from Fisher Scientific (Pittsburgh, PA, USA). Ascorbic acid was purchased from Sigma Aldrich (St. Louis, MO, USA). ^{64}Cu was produced by the PET Department, NIH (Bethesda, MD, UA). Deionized (DI) water with a resistivity of 18.0 MΩ was obtained from a Millipore Autopure system (EMD Millipore, Billerica, MA, USA).

Instruments

Transmission electron microscopy (TEM) imaging was performed on a FEI Tecnai 12 (120 kV). The samples were prepared by depositing a diluted dispersion of liposomes on carbon-coated copper grids, absorbing excess liquid with blotting paper. The hydrodynamic size of liposomes was measured by a Zetasizer Nano series (Zen3600, Malvern). Inductively coupled plasma atomic emission spectroscopy (ICP-AES) was performed on a JY2000 Ultrace ICP atomic emission spectrometer equipped with a JYAS421 auto sampler and 2400 g/mm holographic grating. PET scans were performed using an Inveon PET scanner (Siemens Medical Solutions).

Preparation of liposomes and ^{64}Cu labeled liposomes

The liposomes were prepared according to a method reported previously.[28] Briefly, a lipid mixture was evaporated and dried to a thin film overnight. The lipid film was then hydrated with PBS (pH 7.4) at room temperature with sonication. The solution was then extruded through a polycarbonate filter of 200 nm pore size.

^{64}Cu labeling was performed by modifying a reported method.[33] DOTA was used as a metal chelator and was encapsulated into liposomes during the hydration process. The residual DOTA was removed *via* dialysis. The ^{64}CuCl$_2$ was first added into 2-hydroxyquinoline/HEPES buffer. The DOTA-containing liposomes were then added. After incubation at 25 °C for 1 h, the free ^{64}Cu was separated

from the ^{64}Cu loaded liposome by centrifugal filtration. The labeling efficiency was calculated by instant thin-layer chromatography (ITLC) plates with citric acid (0.1 M pH 5) as an eluent. The labeling efficiency was nearly 80%.

Preparation of ^{64}Cu-labeled Au NRs

Au NRs were modified with SH-PEG-NH$_2$. The ^{64}Cu labeling was carried out following a modified method.[25] Briefly, ^{64}CuCl$_2$ was pre-mixed with sodium ascorbate buffer and vortexed. Au NRs were then added and shaken at 37 °C for 1 h. The resulting ^{64}Cu labeled Au NRs were purified by centrifugal filtration. The labeling efficiency was nearly 100%.

Cell Culture and Animal Model

The U87MG human glioblastoma cells were cultured in MEM medium (Invitrogen, Waltham, MA, USA). The RAW 264.7 cells were grown in DMEM medium (Invitrogen). All cell culture media were supplemented with 10% (v/v) FBS (Gibco, Gaithersburg, MD, USA). All cells were grown at 37 °C under 5% CO$_2$. Athymic nude mice were purchased from Harlan (Indianapolis, IN, USA) and were subcutaneously implanted with 5×10^6 U87MG cells on the right shoulder. The imaging studies were performed 3 weeks after inoculation. Tumor growth was monitored by caliper.

Cell cycles and cell toxicity

The cell viability of different liposomes on RAW cells was estimated by the standard MTT assay using the untreated group as a control. Briefly, the RAW cells were seeded into 96-well plates (10^4 cells per well) overnight. Liposomes were incubated with cells for 24 h. The cells were washed three times with PBS before 10 µL of MTT solution (5 mg/mL) was added. The plate was incubated for another 4 h and washed 100 µL of DMSO was added to dissolve the formazan crystals. The absorbance at 490 nm was measured by a plate reader. The flow cytometric analysis was performed following a standard protocol. Briefly, 10 µM liposomes were incubated with RAW cells for 24 h before cells were washed with PBS, trypsinized, harvested, and centrifuged. The cells were incubated with 5 µL of 2 mg mL^{-1} RNase for 1 h, followed by staining with 75 µL propidium iodide (PI, 1 mg mL^{-1}) for 15 min. Measurement was performed on an Accuri C6 flow cytometer (BD, Ann Arbor, MI, USA) with 488 nm excitation. The data were analyzed by FlowJo version 7.6.5 (FlowJo, Ashland, OR, USA).

PET Studies

Tumor-bearing mice were anesthetized using isoflurane/O$_2$ (2% v/v) and injected intravenously with 2.96-3.7 MBq (80-100 µCi) of ^{64}Cu labeled liposome or Au NRs in a volume of 100 µL PBS. PET scans at different time points for ^{64}Cu labeled liposomes and Au NRs were obtained respectively. Reconstruction of PET images was done without correction for attenuation or scatter using a 3-D ordered subsets expectation maximization algorithm. Image analysis was performed by ASI Pro VMTM software. Regions of interest were drawn on the coronal images to calculate %ID/g, assuming a density of 1 for all tissues.

Ex vivo histological staining

Tissues were fixed in a 4% formaldehyde solution at room temperature. Hematoxylin and eosin (H&E) staining (by BBC Biochemical, Mount Vernon, WA, USA) was observed on a BX41 bright field microscopy (Olympus, Waltham, MA, USA).

Statistical Analysis

Results were presented as mean ± standard deviation (SD). Group comparisons were made using Student's t test for unpaired data. P values < 0.05 were considered statistically significant.

Results and Discussion

Influence of liposomes on cellular uptake of Au NRs

It is well-known that liposomes with diameters larger than 200 nm have high RES uptake and therefore should exhibit good RES blockade effect [6, 27]. However, there is still no consensus on how the surface charges of liposomes affect RES blocking efficiency.

Thus, we prepared liposomes around 200 nm with different surface charges. The liposomes were synthesized *via* a thin film hydration method, followed by several rounds of extrusion [28]. The surface charge was controlled by adjusting the lipid composition: 1, 2–dipalmitoyl-sn-glycero-3-phos-phocholine (DPPC)/cholesterol (CHOL) (8:2) for uncharged (neutral) liposomes, DPPC/1,2-dipalmitoyl-sn-glycero-3-phosphoglycerol (DPPG)/ CHOL (7:1:2) for negative liposomes, and DPPC/1,2-dipalmitoyl-3-trimethylammonium-propane (DPTAP)/ CHOL (7:1:2) for positive liposomes. As shown in **Figure 1**, all three kinds of liposomes have similar morphology and hydrodynamic size (189.9 ± 1.0, 195.1 ± 1.7 and 194.4 ± 1.4 nm, respectively), whereas the zeta potential measurement demonstrated that they were uncharged (0 ± 1.8 mV), negative (-78.1 ± 2.2 mV), or positive (57.5 ± 1.7 mV).
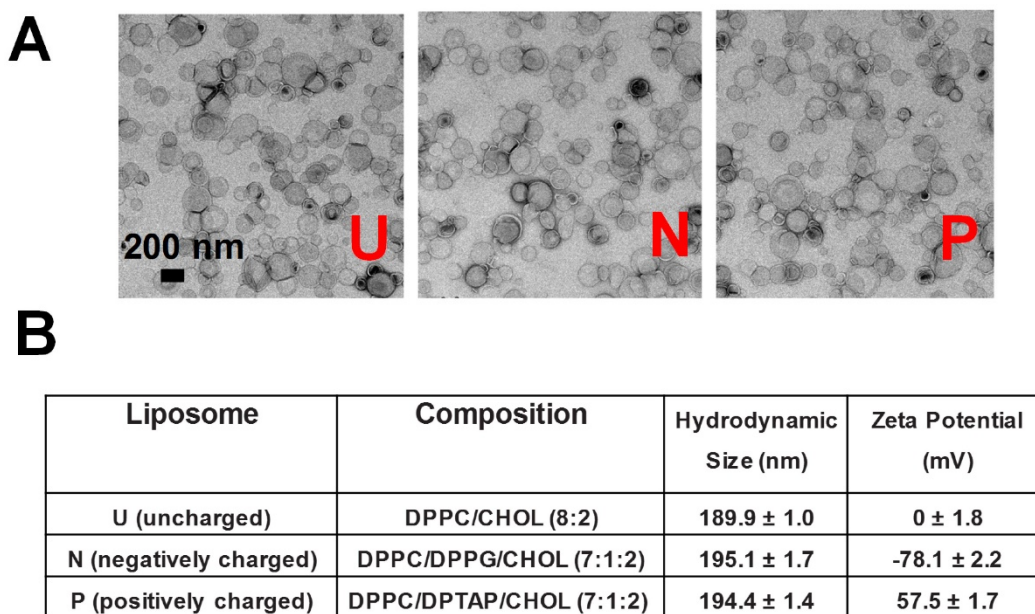
Figure 1. (A) TEM imaging and (B) detailed information on liposomes with different surface charges (neutral/uncharged, negative, positive). DPPC: 1,2-dipalmitoyl-*sn*-glycero-3-phosphocholine; DPPG: 1,2-Dipalmitoyl-sn-glycero-3-phosphoglycerol; DPTAP: 1,2-dipalmitoyl-3-trimethylammonium-propane.
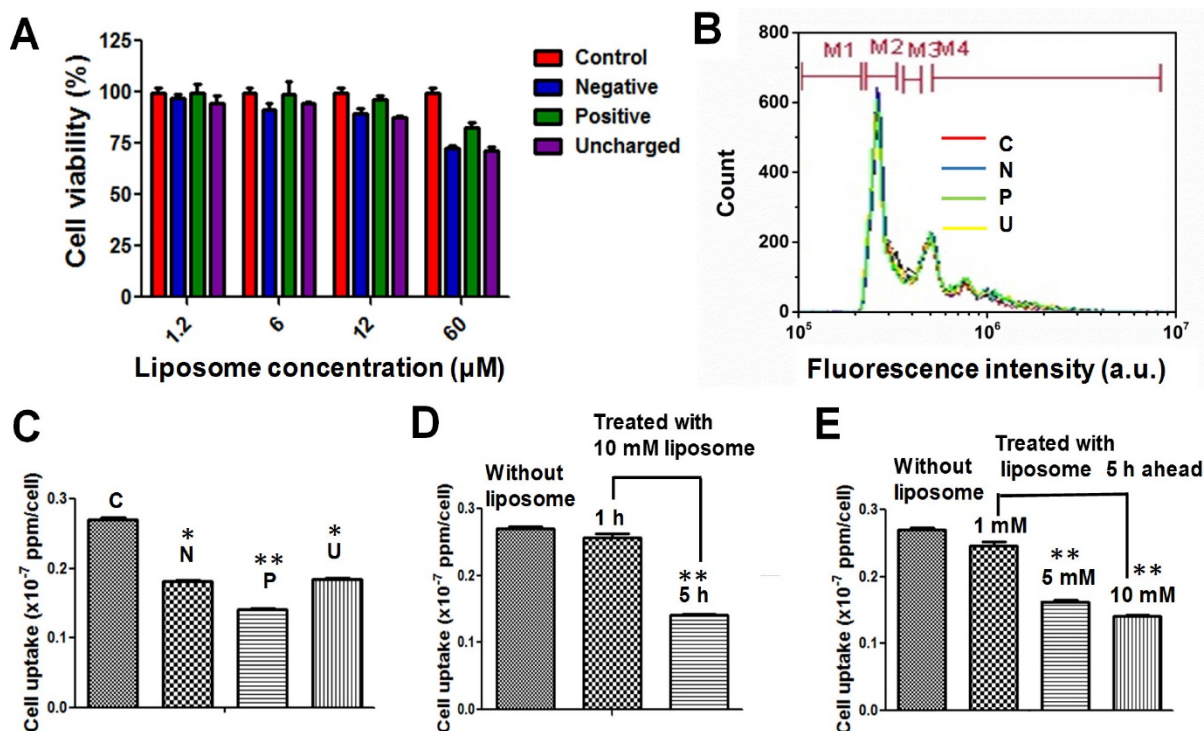

Figure 2. (A) Cell viability and (B) flow cytometry analysis of RAW 264.7 cells after being treated with liposomes of differing surface charge. (C-E) Cell uptake efficiency of Au NRs after 24 h with: (C) pretreatment with different liposomes at a concentration of 10 μM and a time interval of 5 h; (D) pretreatment with 10 μM positive liposomes and different time intervals (1 and 5 h); (E) pretreatment with positive liposomes of different concentrations (1, 5 and 10 μM) and a time interval of 5 h. *P < 0.05, **P < 0.01 compared to without liposome treatment.

The cytotoxicity of all three kinds of liposomes on a common mouse macrophage cell line (RAW 264.7) was assessed to confirm their biocompatibility. At 10 μM liposome, no significant toxicity was observed after 24 h (**Figure 2A**). The flow cytometry analysis further confirmed that 10 μM liposomes, whether positive, negative, or neutral, have negligible influence on the cell cycle (**Figure 2B**). This is consistent with previous observations that liposome-mediated RES blockade does not damage the macrophages or impair liver function [23, 29].

We further investigated the influence of liposomes on the cellular uptake of Au NRs. It has been reported that liposomes can affect the second

dose of NMs in two ways: 1) The liposomes can saturate the receptors on macrophages for foreign particle recognition [30, 31]; 2) The liposomes can deplete the opsonins from plasma, which is important for macrophages to recognize and engulf foreign particles [32]. Thus far, there has been virtually no quantitative study on the extent to which the liposome blockade can decrease cellular uptake of a secondary dose of NMs. We compared the blockade effect of liposomes with different charges at the same dose (10 µM) and the same time interval (5 h). Briefly, we first treated RAW 264.7 cells with 10 µM liposomes, followed by Au NRs 5 h later. The cellular uptake of Au NRs was quantified after 24 h incubation *via* inductively coupled plasma-atomic emission spectroscopy (ICP-AES) measurement. As shown in **Figure 2C**, all three kinds of liposomes demonstrated blockade effects, while the positive liposomes were the most efficient ones, resulting in a dramatic decrease in cellular uptake of Au NRs from $0.270 \pm 0.005 \times 10^{-7}$ ppm/cell to $0.141 \pm 0.005 \times 10^{-7}$ ppm/cell. Focusing on positive liposomes, we then further studied the blockade effect at different time intervals (1 and 5 h) and with various liposome doses (1, 5 and 10 µM). **Figure 2D** demonstrated that 10 µM positive liposomes only slightly blocked the macrophage uptake of Au NRs with a 1 h interval, but could effectively decrease the macrophage uptake to 50% with a 5 h interval. This result indicates the time dependent nature of liposomes to either saturate the receptors on macrophages or to deplete the opsonins. The blockade effect is also liposome concentration dependent. As the liposome dose increased from 1 µM to 5 µM, the blockade efficiency increased from 12% to 41%. However, further increasing the concentration to 10 µM did not further reduce cellular uptake of Au NRs. It might be reasoned that 5 µM is sufficient for receptor saturation and opsonin depletion.

In vivo behavior of liposomes

At the cellular level, positive liposomes exhibited the best macrophage blocking effect. To better predict the *in vivo* blockade effect, we then studied the *in vivo* biodistribution of different liposomes, emphasizing the liver and spleen where the macrophages mainly reside. 64Cu-based PET imaging was used to monitor the distribution of liposomes over time. PET imaging permits non-invasive, direct, and quantitative measurement of specific regions of interest (ROIs) with high sensitivity, and thus is one of the best approaches to study the biodistribution of NMs. 64Cu is an isotope which can produce high quality PET images. Advantageously, its half-life (around 12.7 h) allows for studies even 24 h after administration. We used a method called "remote loading" to label

liposomes with 64Cu [33]. Briefly, DOTA (1,4,7,10-tetraazacyclododecane-1,4,7-triyl) triacetic acid) chelator molecules were encapsulated by liposomes. Then the lipophilic transporter (2-hydroxyquinoline) was complexed with 64Cu to form a labile complex which could enter the liposomes. Transchelation occurred upon introduction of the labile 64Cu complex to the strong hydrophilic chelator DOTA. A stable 64Cu-DOTA complex was formed, entrapped within the liposome cavity as shown in **Figure 3A**. This method of loading has two major advantages: 1) It can be applied to all three kinds of liposomes without the need of chemical functional groups for chelator conjugation on the surface of liposomal structure; 2) It provides high *in vivo* radiochemical stability with 64Cu entrapped within the inner core of liposomes. After 64Cu labeling, no obvious change in size, morphology, or zeta potential was observed.

FVB mice were injected by tail vein with the same amount of 64Cu-labeled liposomes (neutral, positive, and negative) and then underwent PET scanning. It is evident from **Figure 3B** that most liposomes accumulated in the liver and spleen (**Figure 3B**) and were cleared from the blood circulation within 8 h after injection. The spleen had about 30 %ID/g uptake for all three samples at 8 h post-injection. The liver uptakes of neutral and negative liposomes were similar (around 30 %ID/g), while the positive liposomes showed much higher liver accumulation over 60 %ID/g. Our results showed that positive liposomes have the highest liver and spleen targeting ability and should be the most promising candidate for RES blockade.

We then explored the *in vivo* blockade effect of different kinds of liposomes by quantitatively comparing the whole-body distribution of Au NRs after the blockade. Unlabeled liposomes (100 µmol/kg) were injected intravenously into U87MG tumor-bearing mice and 5 h later, 64Cu-labeled Au NRs were injected. The 64Cu-Au NRs were prepared following a well-established method so that the PET signal could accurately locate Au NRs. Visual evaluation of representative whole-body PET images of mice observed slightly higher tumor uptake and less liver or spleen uptake with positive liposome blocking (**Figure 4A**).

The detailed ROI analysis of 64Cu-Au NRs in different tissues were summarized in **Figure 4B-E**. Since 200 nm liposomes were cleared by the RES system and metabolized quickly, the blocking effect is transient and only effective during the first few hours as reported in other studies [29, 34]. Thus, we focused our studies on the first 8 h. All three kinds of liposomes decreased liver (**Figure 4C**) and spleen

(**Figure 4D**) uptake of Au NRs to some extent. Correspondingly, the amount of NRs remaining in the blood of pretreated mice increased (**Figure 4B**) as the RES mediated clearance reduced. The positive liposomes seemed to have the best blockade effect with the liver uptake of NRs decreased from 42.1 ± 5.9 %ID/g to 27.1 ± 2.2 %ID/g, spleen uptake decreased from 23.8 ± 1.0 %ID/g to 14.0 ± 1.0%ID/g, heart signal increased from 12.3 ± 0.4 %ID/g to 27.2 ± 2.2 %ID/g, and tumor uptake increased from 9.3 ± 1.1 %ID/g to 13.6 ± 1.6 %ID/g at 6 h post-injection. The *in vivo* effect of macrophage blockade was not as remarkable as that of the cellular level since the circulation, distribution, as well as metabolism of liposomes and Au NRs all influence the Au NRs' behavior after liposome blockade. Thus, direct *in vivo* monitoring of NMs is of great significance to elucidating the biological fate of NMs in order to guide the rational design of theranostic NMs.

Uptake of Au NRs as a function of liposome dosage and time interval between liposome dose and NR dose.

We further explored the effect of liposome dosage and the time interval between liposome dose and the second NR dose to optimize the blockade efficiency. Following 100 µmol/kg liposome 1 h before injection of Au NRs as an example, the spleen uptake of Au NRs was around half of the unblocked group at 1 h post-injection (12.0 ± 1.3 %ID/g *vs.* 24.6 ± 1.4 %ID/g while the liposome blockade effect on liver was not obvious until 2 h post-injection (29.3 ± 0.6 %ID/g *vs.* 36.0 ± 2.3 %ID/g). It is worth mentioning that for all the mice (both blocked and unblocked groups), the signals in the liver and spleen decreased after 20 h, probably due to the metabolism of NRs. However, the spleen uptake of the blocked group was maintained around 50% (6.6 ± 0.4 %ID/g *vs.* 14.8 ± 0.7 %ID/g) and liver uptake was around 66.7% (18.1 ± 1.3 %ID/g *vs.* 27.9 ± 2.0 %ID/g) of the unblocked group at 27 h post-injection. As liposome pretreatment successfully prevented RES clearance of the second dose of NRs, the heart signal was nearly twice that of the unblocked group (26.5 ± 5.1 %ID/g *vs.* 12.3 ± 0.4 %ID/g at 8 h post-injection.), indicating enhanced blood circulation. Although the heart signal gradually decreased to the same level at the 24 h time point (3.3 ± 0.5 %ID/g *vs.* 3.1 ± 0.8 %ID/g), the enhanced blood half-life (from 9.24 h to 14.35 h) benefited tumor accumulation (from 11.5 ± 1.1 %ID/g to 13.4 ± 0.5 %ID/g) (**Figure S1**).

Figure 5 and **Table 1** compared the effect of pre-injection with different doses (100, 200 and 400 µmol/kg) of unlabeled liposomes on the subsequent tissue distribution of ^{64}Cu-labeled Au NRs. The first dose of liposomes and the second dose of Au NRs were separated by 1 h and 5 h respectively (**Table S1 and Table S2**). It can be seen that liposomes blocked
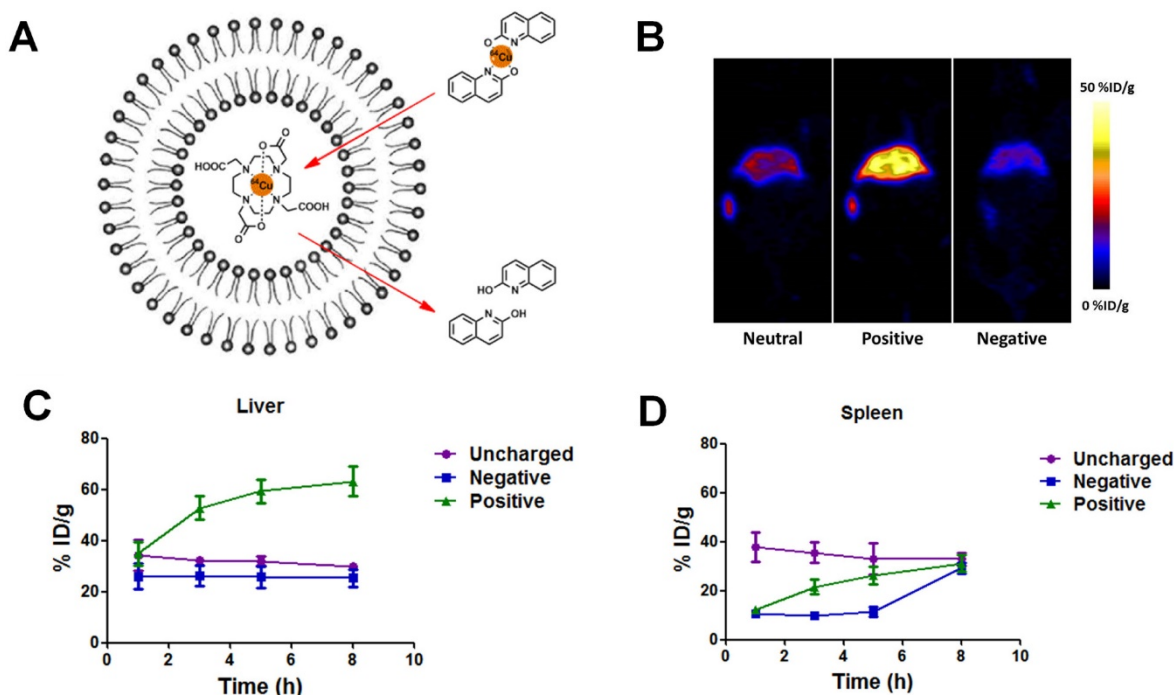

Figure 3. (A) Schematic illustration of ^{64}Cu remote labeling of liposomes. In this approach, 2-hydroxyquinoline served as an ionophore to carry ^{64}Cu across the membrane of liposomes and deliver it to the strong copper chelator DOTA, pre-encapsulated in the liposomes. (B) Representative coronal PET images of mice at 5 h post-injection of 100 µCi neutral, positive and negative liposomes. (C-D) Percentage of injected dose (%ID) of ^{64}Cu-labeled liposomes in spleen (C) and liver (D) over time.

the RES activity in all the groups with a similar trend as described above. For groups with different liposome doses, there was no significant difference in the liver and spleen uptakes of Au NRs. The tumor uptakes of Au NRs were 14.9 ± 1.4 %ID/g, 15.2 ± 1.1 %ID/g, and 16.1 ± 1.3 %ID/g at 27 h post-injection for the 5 h pretreatment interval and 13.4 ± 0.5 %ID/g, 13.9 ± 0.5 %ID/g and 14.9 ± 2.0 %ID/g for the 1 h pretreatment interval as the liposome dosage increased from 100 to 200 and 400 μmol/kg, respectively. For groups with different time intervals, the liver and spleen uptakes were also similar. The tumor uptakes of Au NRs at 27 h post-injection were

slightly higher with 5 h pretreatment interval than those with 1 h pretreatment interval using an equivalent dose of Au NRs. In order to exclude the possibility of detachment of ^{64}Cu from the Au NRs, which might give false indications of Au NR localization, we further sacrificed the mice after the *in vivo* PET imaging study at 27 h and quantified Au amount in the tissue homogenate *via* ICP-AES measurement. The result (**Figure 6**) was consistent with that obtained from PET imaging, confirming the reliability of PET monitoring.
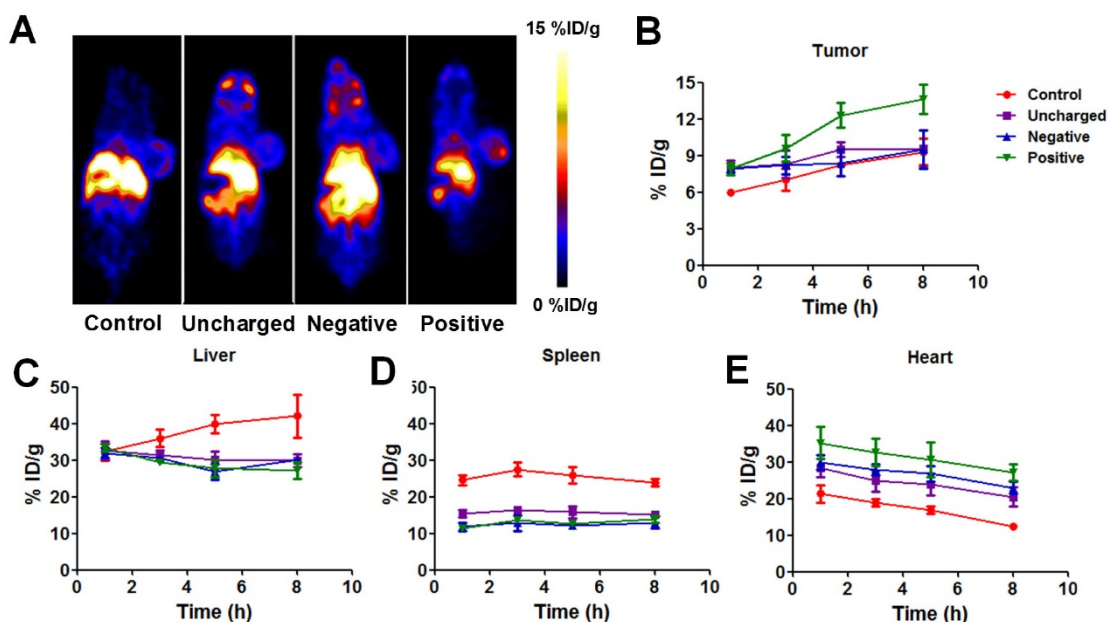

Figure 4. (A) Representative whole-body coronal PET images of U87MG tumor-bearing mice at 5 h after intravenous injection of 100 μCi ^{64}Cu-labeled Au NRs with or without pretreatment of 100 μg negative, neutral, or positive liposomes. (B-E) Quantitative region-of-interest (ROI) analysis of tumor (B), liver (C), spleen (D), and heart (E) uptake of ^{64}Cu-Au NRs over time (n = 3/group) with or without pretreatment of 100 μg negative, neutral, or positive liposomes.

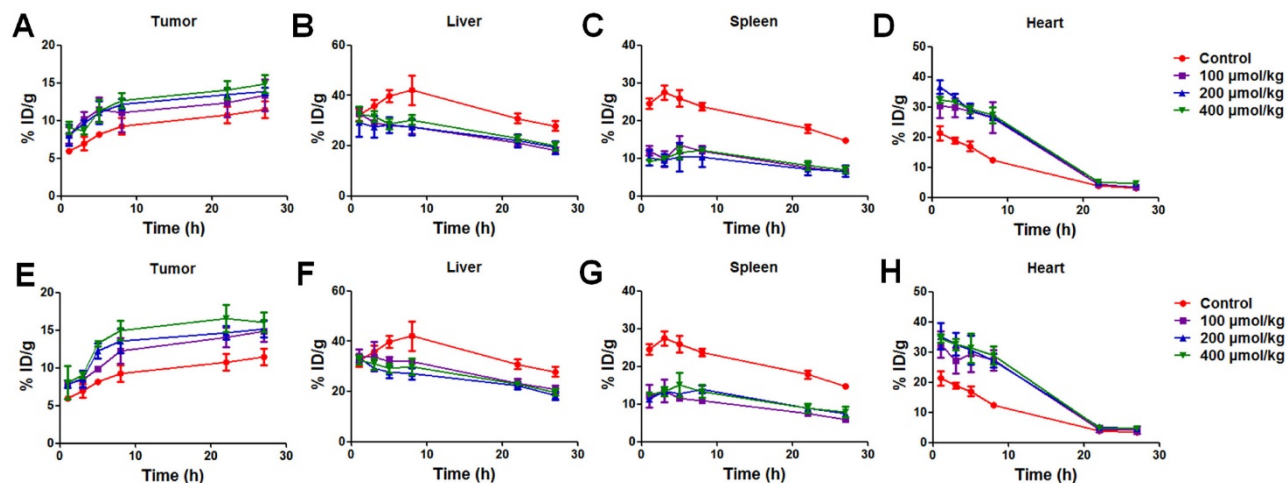**Figure 5.** (A-D) Tissue distribution of ^{64}Cu-labeled Au NRs over time (n = 3/group) following 1 h post-injection of liposomes at different concentrations. (E-H) Tissue distribution of ^{64}Cu-labeled Au NRs 5 h post-injection of liposomes at different concentrations.

Table 1. Effect of pretreatment with positive liposomes on tissue distribution and blood circulation half-life of a second dose of ^{64}Cu-labeled Au NRs.

		Half-life (h)	Tumor uptake (27 h, %ID/g)	Liver uptake (27 h, %ID/g)	Spleen uptake (27 h, %ID/g)
Without liposome blockade		9.24	11.5±1.1	27.9±2.0	14.8±0.7
1 h liposome pretreatment	100 µmol/kg	14.35	13.4±0.5	18.1±1.3	6.6±0.4
	200 µmol/kg	15.39	13.9±0.5	19.3±2.5	6.6±1.5
	400 µmol/kg	15.53	14.9±2.0	19.9±1.6	7.0±0.9
5 h liposome pretreatment	100 µmol/kg	14.25	14.9±1.4	20.9±1.4	5.9±0.6
	200 µmol/kg	15.50	15.2±1.1	18.4±1.7	7.6±0.6
	400 µmol/kg	15.53	16.1±1.3	19.8±1.4	7.9±1.4
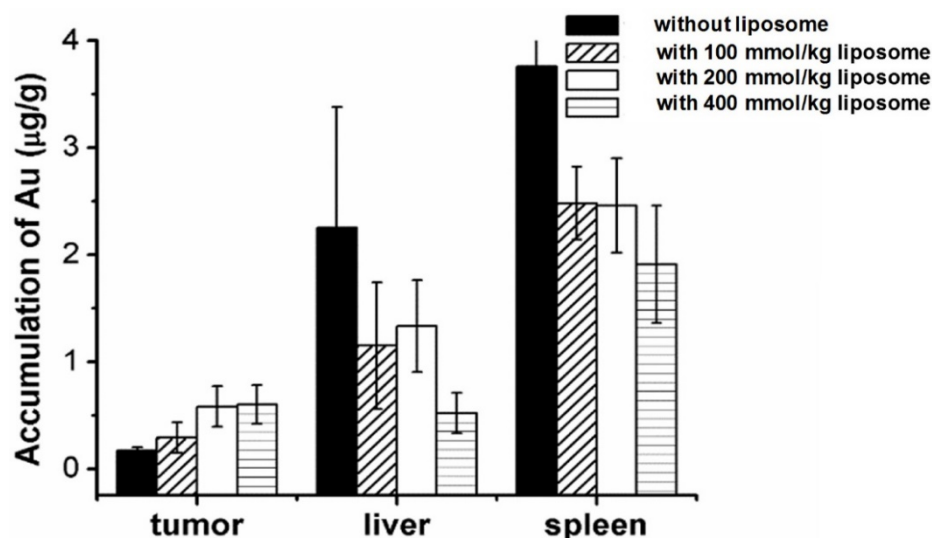
Figure 6. Biodistribution of Au NRs in different tissues based on ICP measurement. The liposomes were injected 5 h in advance to block the RES uptake.

Although we observed an obvious concentration and time interval dependent trend of the liposome blockade at the cellular level, the *in vivo* result did not completely follow the same trend. Taking the liposome dosage as an example, in the present work, we chose three concentrations (100, 200 and 400 µmol/kg). We observed only slight increase of tumor uptake as the dosage increased at the 1 h time interval, but relatively higher tumor accumulation of Au NRs at the time interval of 5 h. It is understandable since the *in vivo* clearance of Au NRs is the result of many different competing processes. For instance, disassembly of liposomes could induce some changes in the physiological state of mice and therefore affect the circulation and metabolism of the following Au NR administration [35]. Moreover, the dynamic evolution of the biological identity of Au NRs and liposomes during circulation may have some effect on the observed *in vivo* behaviors [36]. In another work, liposomes at a higher concentration of 1250 µmol/kg showed even less reduction in the RES clearance rate of carbon than that at 250 µmol/kg. The authors claimed that the uptake of large amount of lipids could inhibit the phagocytic activity and stimulate the RES clearance of carbon [29].

It is of note that at the highest dose used in the present work (400 µmol/kg), liposomes had little apparent toxicity to mice with no observation of behavioral changes or weight loss. There was also no sign of damage to major organs (especially liver and spleen) based on the hematoxylin and eosin staining results (**Figure S1**). However, it is well known that positive liposomes could induce TNF-α secretion and can exert toxicity at high concentrations. Thus, to balance the possible side effects associated with high liposome concentration with the extent of decrease in RES uptake, it seems that 100 µmol/kg, within practical clinical usage parameters, is sufficient for achieving RES blockade.

Liposome based RES blockade strategy

Among all the techniques that have been reported to reduce the nonspecific uptake of NMs by the liver and spleen, the liposome based RES blockade strategy has at least three advantages: first, it is a general approach to improve the circulation of NMs without altering themselves. Since the theranostic properties of NMs are highly dependent on their size, morphology, and surface chemistry [4], it is desirable to maintain their original physicochemical properties.

Second, unlike most RES blockers, the effect of liposome blockade is temporary and reversible with little damage to healthy organs and generally considered as safe in the clinic. Third, the strategy is easy to handle and potentially cost and time-saving.

The effect of pretreatment with liposomes on tissue distribution of a second dose of similar liposomes has been quantitatively evaluated [22, 37]. It has also been reported that the same strategy worked for iron oxide nanoparticles [23] or carbon [29], evidenced by qualitative or semi-quantitative comparison. Meanwhile, several authors reported that they did not observe RES depression following a primary dose of colloid during a secondary dose of different colloid [38]. They attributed this to the fact that opsonization of the first material did not necessarily cause RES depression of the second material. Although there is no conclusive evidence for this theory, we cannot ignore the possibility that liposome based blockade strategy may have different effect for different NMs. Thus, it is important to explore the liposome blockade effect on specific NMs before this strategy is actually performed.

In the present work, we quantitatively investigated the effectiveness of pre-injection of liposomes to block the RES clearance of a second dose of Au NRs. We labeled liposomes and Au NRs with ^{64}Cu and utilized PET imaging to monitor their real-time *in vivo* behavior. We demonstrated that the positive liposomes have the best liver and spleen blockade efficiency among three differently charged liposomes, likely due to their effective electrostatic interaction with negative cell membrane residues (e.g. phosphatidylserine). The influence of liposome dosage and time interval between two injections do not seem to be highly significant within our test range. Based on our observation, an injected dose of 100 μmol/kg positive liposomes (much less than previous reports [23, 29]) is sufficient for RES blocking, with the liver and spleen uptake of Au NRs decreased by 25% and 52%, respectively. Although more parameters need to be tested before we can ascertain which procedure is most beneficial, our study underlines the fact that various dynamic microenvironments inside the body could greatly influence the RES clearance trends and biodistribution patterns of Au NRs; thus competing with the singular blockade effect of liposomes on macrophages (as shown at cellular level) and resulting in a less predictable estimate of *in vivo* activity.

Meanwhile, we found that the tumor uptake of Au NRs has a relationship with the administered liposome dosage and the time interval between injections. The tumor uptake of Au NMs following injection of 400 μmol/kg liposomes 5 h ahead (16.1 ± 1.3 %ID/g at 27 h post-injection) is 20% higher than the tumor uptake following injection of 100 μmol/kg liposomes 1 h ahead (13.4 ± 0.5 %ID/g at 27 h post-injection). Our results indicate that the extent of tumor uptake enhancement is not necessarily consistent with the extent to which liver and spleen uptake decreases. Although the tumor heterogeneity might influence the results, our observation begs the question whether suppressing RES macrophage activity and consequently enhancing the blood circulation of NMs is the only way this strategy improves the tumor uptake. The biological identity of NMs or the tumor microenvironment might also be affected by lipids released by destabilized liposomes.

As the field of nanomedicine is rapidly expanding with a focus on personalized medicine, refinement of drug delivery technology to work in concert with endogenous biological systems is becoming increasingly relevant. Considering the heterogeneous and dynamic nature of the human body, detailed studies are required to identify the *in vivo* effectiveness of strategies influencing NM delivery. PET imaging proves to be a very important quantitative tool to monitor the biological fate of NMs and to understand the biological mechanisms that will guide the selection of procedures suitable for personalized medicine in the future.

Supplementary Material

Supplementary figures and tables.
http://www.thno.org/v07p0319s1.pdf

Acknowledgment

Competing Interests

The authors have declared that no competing interest exists.

References

1. Min Y, Caster JM, Eblan MJ, Wang AZ. Clinical Translation of Nanomedicine. Chem. Rev. 2015; 115: 11147-11190.
2. Wicki A, Witzigmann D, Balasubramanian V, Huwyler J. Nanomedicine in Cancer Therapy: Challenges, Opportunities, and Clinical Applications. J. Control. Release 2015; 200: 138-157.
3. Caruso F, Hyeon T, Rotello VM. Nanomedicine. Chem. Soc. Rev. 2012; 41: 2537-2538.

4. Lim EK, Kim T, Paik S, Haam S, Huh YM, Lee K. Nanomaterials for Theranostics: Recent Advances and Future Challenges. Chem. Rev. 2014; 115: 327-394.
5. Ma X, Zhao Y, Liang XJ. Theranostic Nanoparticles Engineered for Clinic and Pharmaceutics. Acc. Chem. Res. 2011; 44: 1114-1122.
6. Ilium L, Davis S, Wilson C, Thomas N, Frier M, Hardy J. Blood Clearance and Organ Deposition of Intravenously Administered Colloidal Particles. The Effects of Particle Size, Nature and Shape. Int. J. Pharm. 1982; 12: 135-146.
7. Petros RA, DeSimone JM. Strategies in the Design of Nanoparticles for Therapeutic Applications. Nat. Rev. Drug Discov. 2010; 9: 615-627.
8. Wilhelm S, Tavares AJ, Dai Q, Ohta S, Audet J, Dvorak HF, et al. Analysis of Nanoparticle Delivery to Tumours. Nat. Rev. Mater. 2016; 1: 16014.
9. Wang B, He X, Zhang Z, Zhao Y, Feng W. Metabolism of Nanomaterials in vivo: Blood Circulation and Organ Clearance. Acc. Chem. Res. 2012; 46: 761-769.
10. Yu M, Zheng J. Clearance Pathways and Tumor Targeting of Imaging Nanoparticles. ACS Nano 2015; 9: 6655-6674.
11. Ehlerding EB, Chen F, Cai W. Biodegradable and Renal Clearable Inorganic Nanoparticles. Adv. Sci. 2016; 3: 1500223.
12. Liu J, Yu M, Zhou C, Zheng J. Renal Clearable Inorganic Nanoparticles: a New Frontier of Bionanotechnology. Mater. Today 2013; 16: 477-486.
13. Benezra M, Penate-Medina O, Zanzonico PB, Schaer D, Ow H, Burns A, et al. Multimodal Silica Nanoparticles are Effective Cancer-Targeted Probes in a Model of Human Melanoma. J. Clin. Invest. 2011; 121: 2768-2780.
14. Phillips E, Penate-Medina O, Zanzonico PB, Carvajal RD, Mohan P, Ye Y, et al. Clinical Translation of an Ultrasmall Inorganic Optical-PET Imaging Nanoparticle Probe. Sci. Trans. Med. 2014; 6: 260ra149-260ra149.
15. Patel KR, Li MP, Baldeschwieler JD. Suppression of Liver Uptake of Liposomes by Dextran Sulfate 500. Proc. Natl. Acad. Sci. U S A 1983; 80: 6518-6522.
16. Tanaka T, Taneda K, Kobayashi H, Okumura K, Muranishi S, Sezaki H. Application of Liposomes to the Pharmaceutical Modification of the Distribution Characteristics of Drugs in the Rat. Chem. Pharm. Bull 1975; 23: 3069-3074.
17. Diagaradjane P, Deorukhkar A, Gelovani JG, Maru DM, Krishnan S. Gadolinium Chloride Augments Tumor-Specific Imaging of Targeted Quantum Dots in vivo. ACS Nano 2010; 4: 4131-4141.
18. Van Rooijen N, Van Nieuwmegen R. Elimination of Phagocytic Cells in the Spleen after Intravenous Injection of Liposome-Encapsulated Dichloromethylene Diphosphonate. Cell Tissue Res. 1984; 238: 355-358.
19. Allen TM, Cullis PR. Liposomal Drug Delivery Systems: from Concept to Clinical Applications. Adv. Drug Deliv. Rev. 2013; 65: 36-48.
20. Pattni BS, Chupin VV, Torchilin VP. New Developments in Liposomal Drug Delivery. Chem. Rev. 2015; 115: 10938-10966.
21. Lian T, Ho RJ. Trends and Developments in Liposome Drug Delivery Systems. J. Pharm. Sci. 2001; 90: 667-680.
22. Abra RM, Bosworth M, Hunt C. Liposome Disposition in vivo: Effects of Pre-dosing with Lipsomes. Res. Commun. Chem. Pathol. Pharmaco. 1980; 29: 349-360.
23. Liu T, Choi H, Zhou R, Chen IW. RES Blockade: A Strategy for Boosting Efficiency of Nanoparticle Drug. Nano Today 2015; 10: 11-21.
24. Huang X, Neretina S, El-Sayed MA. Gold Nanorods: from Synthesis and Properties to Biological and Biomedical Applications. Adv. Mater. 2009; 21: 4880-4910.
25. Sun X, Huang X, Yan X, Wang Y, Guo J, Jacobson O, et al. Chelator-Free 64Cu-Integrated Gold Nanomaterials for Positron Emission Tomography Imaging Guided Photothermal Cancer Therapy. ACS Nano 2014; 8: 8438-8446.
26. Song J, Yang X, Jacobson O, Huang P, Sun X, Lin L, et al. Ultrasmall Gold Nanorod Vesicles with Enhanced Tumor Accumulation and Fast Excretion from the Body for Cancer Therapy. Adv. Mater. 2015; 27: 4910-4917.
27. Liu D, Mori A, Huang L. Role of Liposome Size and RES Blockade in Controlling Biodistribution and Tumor Uptake of GM 1-Containing Liposomes. Biochim. Biophys. Acta 1992; 1104: 95-101.
28. Szoka F, Papahadjopoulos D. Procedure for Preparation of Liposomes with Large Internal Aqueous Space and High Capture by Reverse-Phase Evaporation. Proc. Natl. Acad. Sci. U S A 1978; 75: 4194-4198.
29. Ellens H, Mayhew E, Rustum YM. Reversible Depression of the Reticuloendothelial System by Liposomes. Biochim. Biophys. Acta 1982; 714: 479-485.
30. Gregoriadis G, Neerunjun DE. Control of the Rate of Hepatic Uptake and Catabolism of Liposome-Entrapped Proteins Injected into Rats. Possible Therapeutic Applications. Eur. J. Biochem. 1974; 47: 179-185.
31. Gregoriadis G, Neerunjun DE, Hunt R. Fate of a Liposome-Associated Agent Injected into Normal and Tumour-bearing Rodents. Attempts to Improve Localization in Tumour Tissues. Life Sci. 1977; 21: 357-369.
32. Saba TM. Physiology and Physiopathology of the Reticuloendothelial System. Arch. Intern. Med. 1970; 126: 1031-1052.
33. Petersen AL, Binderup T, Rasmussen P, Henriksen JR, et al: 64 Cu Loaded Liposomes as Positron Emission Tomography Imaging Agents. Biomaterials 2011; 32: 2334-2341.
34. Souhami RL, Patel HM, Ryman BE. The Effect of Reticuloendothelial Blockade on the Blood Clearance and Tissue Distribution of Liposomes. Biochim. Biophys. Acta 1981; 674: 354-371.
35. Naudí A, Jové M, Ayala V, Portero-Otín M, Barja G, Pamplona R, et al. Membrane Lipid Unsaturation as Physiological Adaptation to Animal Longevity. Front Physiol. 2013; 4: 372.
36. Mu Q, Jiang G, Chen L, Zhou H, Fourches D, Tropsha A. Chemical Basis of Interactions Between Engineered Nanoparticles and Biological Systems. Chem. Rev. 2014; 114: 7740-7781.
37. Kao YJ, Juliano RL. Interactions of Liposomes with the Reticuloendothelial System Effects of Reticuloendothelial Blockade on the Clearance of Large Unilamellar Vesicles. Biochim. Biophys. Acta 1981; 677: 453-461.
38. Wagner Jr HN, Iio M. Studies of the Reticuloendothelial System (RES). III. Blockade of the RES in Man. J. Clin. Invest. 1964; 43: 1525.